geosciences

Article

Exploring the Influence of Climate Change on Earthen Embankments with Expansive Soil

Debayan Ghosh [1], Aritra Banerjee [1,*], Anand J. Puppala [2] and Prince Kumar [2]

[1] Department of Civil and Environmental Engineering, South Dakota State University, Brookings, SD 57007, USA; debayan.ghosh@jacks.sdstate.edu
[2] Zachry Department of Civil and Environmental Engineering, Texas A&M University, College Station, TX 77843, USA; anandp@tamu.edu (A.J.P.); prince.kumar@tamu.edu (P.K.)
* Correspondence: aritra.banerjee@sdstate.edu; Tel.: +1-605-688-4918

Abstract: Climate change is known to cause alterations in weather patterns and disturb the natural equilibrium. Changes in climatic conditions lead to increased environmental stress on embankments, which can result in slope failures. Due to wetting–drying cycles, expansive clayey soil often swells and shrinks, and matric suction is a major factor that controls the behavior. Increased temperature accelerates soil evaporation and drying, which can cause desiccation cracks, while precipitation can rapidly reduce soil shear strength. Desiccated slopes on embankments built with such soils can cause surficial slope failures after intense precipitation. This study used slope stability analysis to quantify how climate-change-induced extreme weather affects embankments. Historic extreme climatic events were used as a baseline to estimate future extremes. CMIP6 provided historical and future climatic data for the study area. An embankment was numerically modeled to evaluate the effect on slope stability due to the precipitation change induced by climate change. Coupled hydro-mechanical finite element analyses used a two-dimensional transient unsaturated seepage model and a limit equilibrium slope stability model. The study found that extreme climatic interactions like precipitation and temperature due to climate change may reduce embankment slope safety. The reduction in the stability of the embankment due to increased precipitation resulting from different greenhouse gas emission scenarios was investigated. The use of unsaturated soil strength and variation of permeability with suction, along with the phase transition of these earthen embankments from near-dry to near-saturated, shows how unsaturated soil mechanics and the hydro-mechanical model can identify climate change issues on critical geotechnical infrastructure.

Keywords: climate change; slope stability; unsaturated soil mechanics; shared socioeconomic pathways; transient seepage; extreme precipitation

check for updates

Citation: Ghosh, D.; Banerjee, A.; Puppala, A.J.; Kumar, P. Exploring the Influence of Climate Change on Earthen Embankments with Expansive Soil. *Geosciences* **2024**, *14*, 37. https://doi.org/10.3390/geosciences14020037

Academic Editors: Mohamed Shahin and Jesus Martinez-Frias

Received: 16 December 2023
Revised: 26 January 2024
Accepted: 27 January 2024
Published: 30 January 2024

Copyright: © 2024 by the authors. Licensee MDPI, Basel, Switzerland. This article is an open access article distributed under the terms and conditions of the Creative Commons Attribution (CC BY) license (https://creativecommons.org/licenses/by/4.0/).

1. Introduction

Embankments and levees are critical infrastructures that are often impacted by storms and hurricanes. Earthen embankments are used primarily as a means of transportation networks and flood defenses. These act as lifelines for mankind as transportation facilities and river training structures and are often the last form of defense against flooding. The failure of such structures due to extreme climatic events can cause societal and economic disruption [1]. Recently, a levee failed on the Pajaro River in central California that had experienced prolonged periods of drought followed by incessant precipitation. This resulted in mass evacuations and flooding, which highlights the need to study the effects of climate change on critical civil infrastructure [2]. Several factors such as surface erosion, softening of the soil, tensile cracking, soil desiccation, and seismicity can contribute to the failure of a slope [3]. Researchers have illustrated that, for soil slopes, the behavior of the deeper layers is governed by the changing water table, while the surface layers are governed by atmospheric conditions [4]. Climate change can cause a negative effect or even a calamitous effect on the stability of the slope as the slopes are continuously exposed to extreme climatic conditions [5]. It was illustrated that the critical parameters for slope stability are the hydraulic properties, including permeability and water retention, which are highly influenced by environmental factors [5].

Expansive soils are prevalent in arid and semiarid regions worldwide, including Australia, Canada, China, India, South Africa, and the United States. These soils generally display a moderate to high ability to be molded, a low to moderate level of strength, and a high tendency to swell and shrink in volume [6,7]. The weathering by-products of limestone material and alluvial deposits in the North Central Texas region result in moderate- to high-plasticity clayey soils. In this region, the montmorillonite-rich Eagle Ford Shale clay from the upper Cretaceous period is expansive in nature [8]. To mitigate the adverse effects of these soils, different rehabilitation strategies have been employed in the region [9–17]. Untreated forms of expansive soils typically undergo high swell–shrink characteristics with a variation in the moisture regime. Desiccation cracking occurs within the plastic fill materials as a result of repeated drying and wetting cycles [18]. The most important deformation phenomenon of unsaturated soils, and especially expansive soils, is swelling or shrinking [19]. The engineering properties of collapsible, residual, compacted, and expansive soils, which are usually in an unsaturated state, can be better understood by considering the impact of matric suction [20]. Expansive soils have high values of swelling and compression indices and are subject to frequent changes in matric suction ($u_a - u_w$), which causes additional volume changes. A structure constructed on expansive soil is subject to heave or settlement depending on moisture suction fluctuations [20]. Hence, it is crucial to consider the influence of matric suction when evaluating slope stability.

Desiccation cracks develop when the soil can no longer withstand the tensile stresses caused by shrinkage [21]. During precipitation, water infiltrates the soil through these cracks. Infiltration elevates the pore water pressure, leading to a subsequent decrease in the shear strength of the soil, which causes failure to occur [22,23]. After prolonged exposure to environmental factors like the wetting–drying cycle, fully softened shear strength eventually develops in clays [24]. Surficial failures may occur abruptly and without warning. At times, they may be accompanied by fissures or other indications of impending failures. A slope demonstrates greater strength in the dry season due to the soil being in an unsaturated state with negative pore water pressure and higher values of matric suction. This can also lead to an overestimation of the factor of safety [25]. Numerous slopes at the desiccated state fail when subjected to intense rainfall due to a decrease in matric suction and an increase in pore water pressures. The impact of climate change may increase the severity and frequency of these issues, which may be modeled by incorporating the climate prediction models in the slope stability analysis. The soil–water characteristic curve establishes the relationship between the volumetric water content of the soil and the matric suction, which, in turn, determines the failure mechanism. The phenomenon is influenced by the flux boundary conditions, specifically rainfall infiltration, evaporation, and evapotranspiration at the interface between the soil and the atmosphere [26]. The increased rainfall can cause failure in earthen structures [27,28]. In addition to the intensity of rainfall, other factors such as the characteristics of rainfall, previous precipitation, soil properties, and topography also play a role in the failure of a slope [29]. This issue becomes amplified when we consider the distress in expansive soils caused by drought-like conditions [17,30,31]. Any drought-like condition followed by intense precipitation can cause severe damage to earthen structures, which are anticipated to be negatively impacted by climate change [31–33]. Figure 1 shows the interaction between climatic conditions and expansive slope and the subsequent formation of desiccation cracks due to shrinkage–swelling, which ultimately leads to surficial failure. Climate change may also affect agricultural productivity through higher soil erosion, which may occur due to higher-intensity storms, floods, and the exposure of deeper layers due to the formation of desiccation cracks in expansive soils during prolonged periods of drought. Therefore, there is an urgent need to study the behavior of embankments when subjected to stresses caused by climate change.

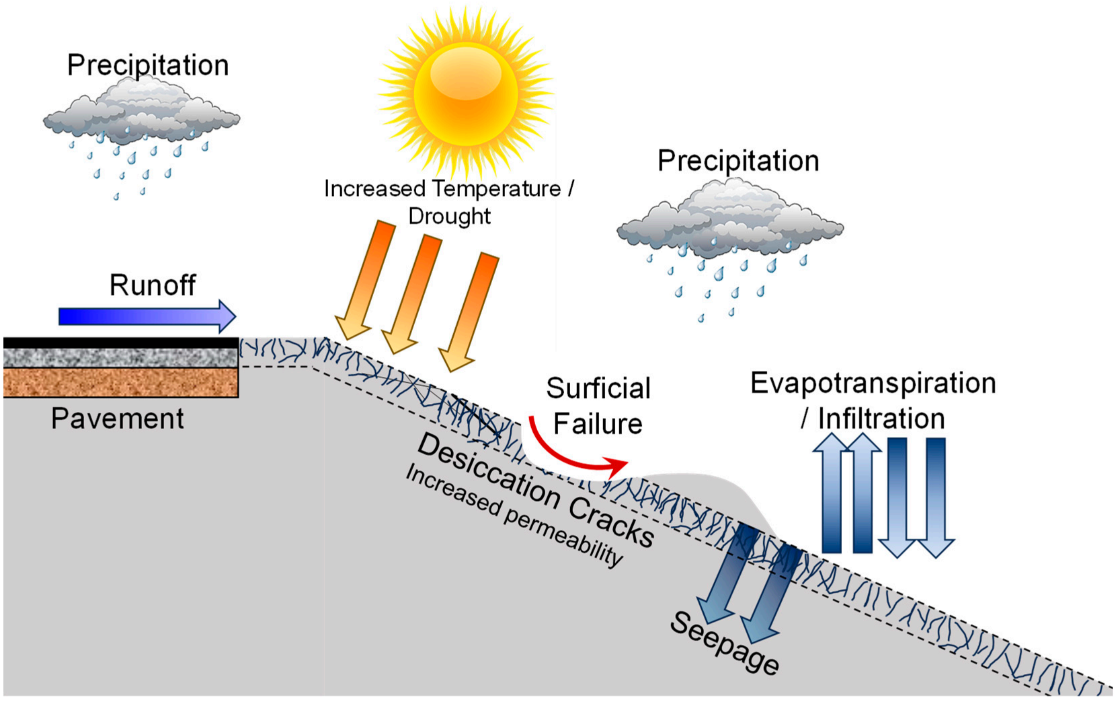

Figure 1. Schematic of climatic interactions with slope and surficial failure.

Incorporating Climate Change Data in Geotechnical Engineering

The advancement in climate and geotechnical modeling has enabled the measurement of the effects of climate change on geotechnical infrastructures. Assessing the impact of climate change on the stability of slopes and embankments involves analyzing three intricate processes: (a) forecasting more detailed future climate data, (b) calculating pore water pressures (PWPs) in slopes caused by changes in variables due to climate conditions, and (c) estimating the factor of the safety of slopes based on the calculated PWPs. Coupled hydro-mechanical finite element analysis can be used for the slope stability analysis of expansive clay embankments. Researchers have used this method to consider the characteristics of expansive clay and the presence of desiccation cracks and found an increase in the saturated coefficient of permeability for the surface layer [34–36].

There are several climate models available to predict future climate scenarios. The CMIP6 (Coupled Model Intercomparison Project Phase 6) presents new global climate model data assessed in the AR6 of the IPCC (Intergovernmental Panel on Climate Change). CMIP6 utilizes shared socioeconomic pathways (SSPs) to simulate different socioeconomic scenarios that may be affected by urbanization, population growth, changes in gross domestic product in different nations, and greenhouse gas (GHG) emissions [37]. The CMIP6 models reveal an approximately 6 °C temperature increase and an increase of 10–30% precipitation over the US under the high emission scenario of SSP5–8.5 by the end of the century, which is considered the extreme scenario [38]. The consideration of the increased intensity and frequency of extreme precipitation due to climate change is an important aspect of the design of future infrastructure as well as the stability analysis of existing infrastructure [2,39]. Robinson et al. (2017) conducted a study to examine how future excessive precipitation will affect landslides in a region close to Seattle, Washington, in the United States [40]. The CMIP5 climate dataset was utilized to generate a collection of current and future intensity–duration–frequency (IDF) curves. Though the analysis focused on a specific emission scenario and intensity duration, the findings of their research suggest that the projected climate conditions in the future may have detrimental consequences for future landslides. Additionally, relying solely on historical climate data in design could result in underestimating the potential risks involved [40]. Researchers have examined the impact of climate change on the stability of embankments [41]. The investigators measured the impact of predicted long-term and extreme precipitation events on the potential instability of sandy and silty highway embankments in southern Ontario, Canada. To conduct their analysis, the researchers employed a two-dimensional (2D) transient variably saturated seepage finite element model to examine pore water pressures. Additionally, they utilized a 2D limit equilibrium slope stability model to assess the stability of the model [41]. The work was conducted using the CMIP5 climate dataset, and the climate data were changed with the introduced shared socioeconomic pathways in CMIP6.

The impact of increased mean precipitation and extreme precipitation events due to climate change on the slope stability of an expansive clay embankment in North Central Texas is presented in this study. To consider the effect of climate change, four general circulation models (GCMs) were considered and compared with the climate normals from the National Oceanic and Atmospheric Administration's National Center for Environmental Information (NOAA NCEI) database. Historical and future precipitation data for 30 years of the location were considered in the study for the climate ensemble. A combination of finite-element-based software, SEEP/W from Geostudio version 2023.1.1, and limit-equilibrium-approach-based software, SLOPE/W from Geostudio version 2023.1.1, was used to quantify the stability of the slope in terms of the factor of safety. The FOS of the embankment slope under baseline and future precipitation was analyzed and compared. The impact of fissures and cracks was assessed by utilizing the soil water characteristic curve (SWCC) and hydraulic conductivity function, which incorporates an elevated saturated coefficient of permeability to accurately simulate the surface layer conditions in the in-situ condition. The study presents a framework to effectively quantify the effect of increased precipitation due to climate change on the existing embankment infrastructure. This study also presents a pioneering study of climatic impact on the short-term failure of embankments of expansive soils using the CMIP6 climate dataset, as most of the assessment of the impact of climate change on existing infrastructure was conducted using the previous CMIP5 dataset.

2. Climate Data

2.1. Historical Climate Dataset

Baseline climate (BC) is considered the datum for the climate change impact assessment for this study. The historical precipitation was used to establish the climate model prediction suitable for the location. The 30 years of precipitation data between 1981 and 2010 were considered in the study as the baseline precipitation. The baseline data for the comparison with four General Circulation Models (GCMs) were collected from the NASA Earth Exchange Global Daily Downscaled Projections (NEX–GDDP) data repository. The observed climate normal data were collected from the NOAA NCEI database for the nearest meteorological station of the study location. The rainfall and mean air temperature data with the daily temporal resolution are shown in Figure 2. The comparison of the average daily rainfall for each month with the observed climate normals was conducted as shown in Table 1. Root-mean-square error (RMSE) is a metric used to evaluate the precision of predicted values in relation to the true value. Regression analysis is a statistical technique used to effectively summarize observed data. The coefficient of determination, also known as the R^2 value, quantifies the degree of correlation between two variables [42]. From Table 1, it could be interpreted that some of the GCMs are better suited for the parameters used for comparison. Though the R^2 value of the data from GFDL ESM4 is not the lowest, it has the lowest root-mean-square error (RMSE) and low average annual precipitation error, whereas the CESM2 dataset has a very high percentage of annual precipitation error. Chai and Draxler (2014) demonstrated the use of RMSE for the comparison of climate models [43]. In this study, the data from the Geophysical Fluid Dynamics Laboratory (GFDL), USA, were selected to predict the future climate data. From the climate data, it can be observed that the average annual precipitation was 903.8 mm for over 30 years.

Daily precipitation of 40 mm or higher is considered a heavy precipitation event in this study. As shown in Figure 2, over 30 years, there were 48 days with 40 mm or more daily precipitation. In September 1999, 74.6 mm of precipitation per day was the highest amount ever recorded in the period.

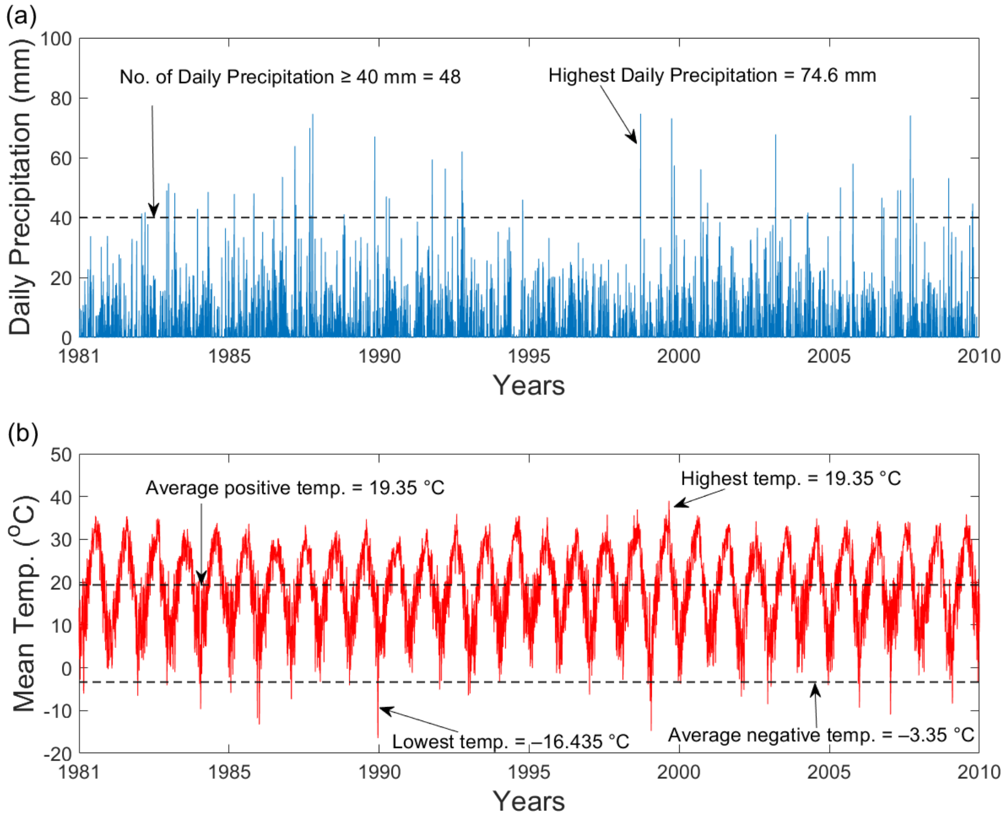

Figure 2. Baseline climatic conditions between 1981 and 2010: (**a**) daily precipitation, (**b**) daily mean temperature.

Table 1. Comparison of different GCMs in relation to baseline climate.

GCM	Modeling Center	RMSE (mm) *	R^2	Percentage Error (Annual)
CESM2	National Center for Atmospheric Research, USA	14.81	0.83	15.26
ACCESS CM2	Australian Community Climate and Earth System Simulator, Australia	13.51	0.73	9.21
GFDL ESM4	Geophysical Fluid Dynamics Laboratory (GFDL), USA	12.68	0.77	8.50
CanESM5	Canadian Centre for Climate Modelling and Analysis, Canada	13.63	0.64	7.69

* RMSE—root-mean-square error.

2.2. Future Climate Dataset

The future climate (FC) data for the site in Texas were collected from the NASA NEX–GDDP [44]. Considering the inherent constraints of climate change models, it is crucial to implement bias adjustment when applying them at the local level. These models, which work at large scales, often fail to accurately capture local climatic variations, leading to systematic inaccuracies or biases. Improving model accuracy by aligning model outputs with observed local climate data through bias correction is essential for making well-informed decisions. Nevertheless, the implementation of this method necessitates prudence in order to prevent the introduction of additional errors. Although bias correction enhances the accuracy of local climate model estimates, it is unable to entirely eradicate all forms of uncertainty [45]. Downscaling techniques are utilized to tackle the low spatial resolution data obtained from Global Climate Models. The NEX GDDP dataset includes downscaled, bias-corrected climate scenarios from the General Circulation Models (GCMs) in $0.25^\circ \times 0.25^\circ$ resolution [45]. The data from the GFDL ESM4 model were collected for SSP2–4.5 and SSP5–8.5 over 2031–2060 and 2071–2100. The 2031–2060 and 2071–2100 years represent the mid-century and end of the century, respectively. The daily precipitation data for these SSPs and periods are shown in Figure 3.

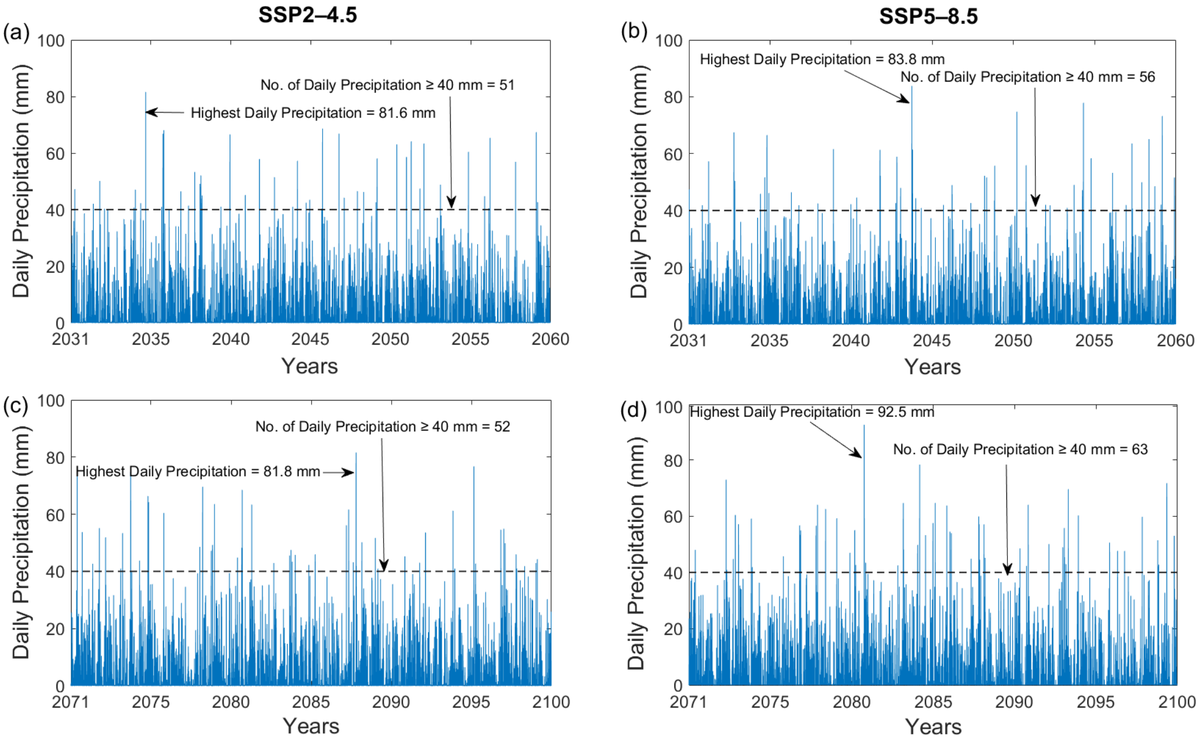

Figure 3. Modeled future daily precipitation from GFDL ESM4 dataset: (**a**) SSP2–4.5 2031–2060, (**b**) SSP5–8.5 2031–2060, (**c**) SSP2–4.5 2071–2100, and (**d**) SSP5–8.5 2071–2100.

As discussed earlier, SSPs are a collection of scenarios created to illustrate possible future changes in human society. SSPs play a crucial role in predicting future levels of greenhouse gas emissions and their effects on climate change. The SSP2 scenario is considered to have moderate challenges to mitigation and adaptation. Environmental systems will undergo degradation, although with some improvements, and there will be an overall decrease in the intensity of resource and energy utilization in SSP2 [46]. The SSP5–8.5 scenario predicts that there will be high levels of greenhouse gas emissions and insufficient efforts to mitigate climate change. SSP5–8.5 may lead to a global temperature increase of 4–6 °C above pre-industrial levels by the end of the century. The scenario also predicts a peak radiative forcing of 8.5 W/m^2 before a subsequent decrease [47]. It can be observed from Figure 3a,c that, for SSP2–4.5, the number of extreme precipitation events does not increase significantly with time.

2.3. Extreme Events

For most of the climate data repository, the data are often limited to daily resolution, but the intensity of precipitation can fluctuate from minutes to hours. The precipitation data resolution for NEX GDDP was daily. The historical extreme precipitation events were compared to the DDF curves to address the effects of the temporal resolution of precipitation and more plausible resolutions were chosen. An intensity–duration–frequency curve was converted to a DDF curve for a selected period [41]. The DDF curve for the embankment location is shown in Figure 4 and was obtained from the National Oceanic and Atmospheric Administration (NOAA) Atlas 14. As the 30-year climatic ensemble is considered for the study, the return period of the extreme precipitation for the highest rainfall is considered to be 30 years and the duration of the event is estimated using the DDF curve.

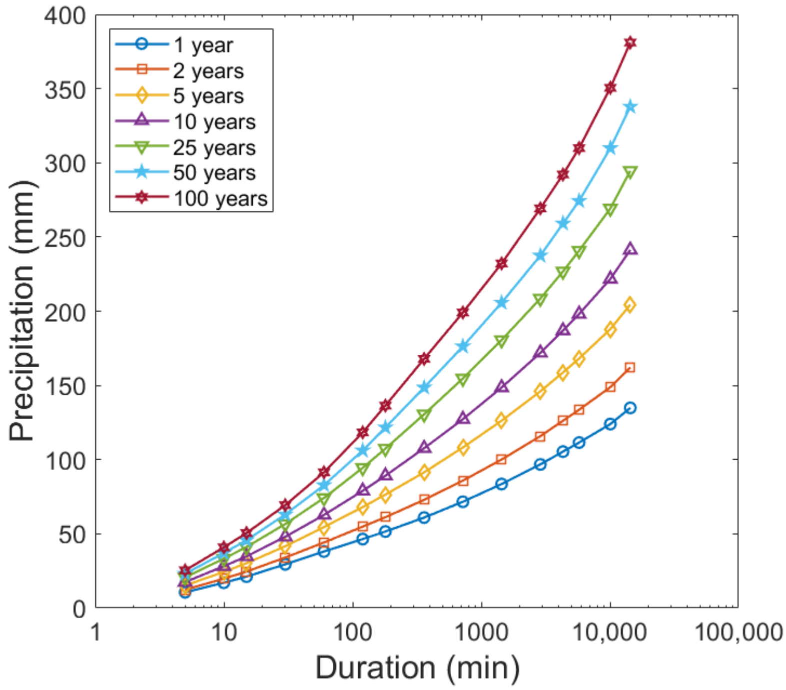

Figure 4. Depth–duration–frequency curves for the site.

3. Numerical Modeling and Analysis

3.1. Soil Properties

Most of the soil data was obtained from various experiments and studies conducted by the authors and their research groups. The SWCC data of the soil are presented in Figure 5. The SWCC was determined using the filter paper method and a chilled mirror hygrometer. The closed-form solution proposed by the Fredlund–Xing (FX) (1994) model was used as shown below to fit the experimental data into the SWCC curve [48]. The hydraulic conductivity and volumetric water content in unsaturated soils are dependent on matric suction. The air entry value (AEV) is the critical suction at which soil starts to lose moisture with increasing desaturation. AEV is dependent on the pore spaces and pore structure within the soil. The AEV of this soil at its maximum dry density was determined to be 10 kPa. The saturated volumetric water content and residual volumetric water content were computed to be 0.441 and 0.08, respectively. The unsaturated hydraulic conductivity of the soil was determined based on experimental studies conducted on a modified suction-controlled permeability setup. The soil sample was maintained at a specific suction state, while the hydraulic conductivity was measured after equilibration. The steps were repeated for different suction levels, and the HCF of the soil used in this study is shown in Figure 6. Table 2 shows the soil properties used in the study. For compacted core soil, shear strength parameters were measured using a direct shear test, and a torsional ring shear test was used for the strength parameters of the surface layer.

$$\theta_w = C(\psi)\theta_s \left[\frac{1}{ln\{e + (\frac{\psi}{a})^n\}} \right]^m \tag{1}$$

where θ_w, θ_s, and θ_r are natural, saturated, and residual volumetric water content, respectively, ψ is matric suction, and a, n, and m are the curve fitting parameters. The hydraulic conductivity function from the data in Figure 6 was fitted using the van Genuchten (1980) model, as shown below [49].

$$K(h) = K_s S_e^l [1 - (1 - S_e^{l/m})^m]^2 \tag{2}$$

where K_s is saturated hydraulic conductivity, l is the pore conductivity parameter, S_e is effective saturation, and m represents the curve fitting parameter. Some of the material properties for this study were collected from experiments conducted in several studies [18,25,50].

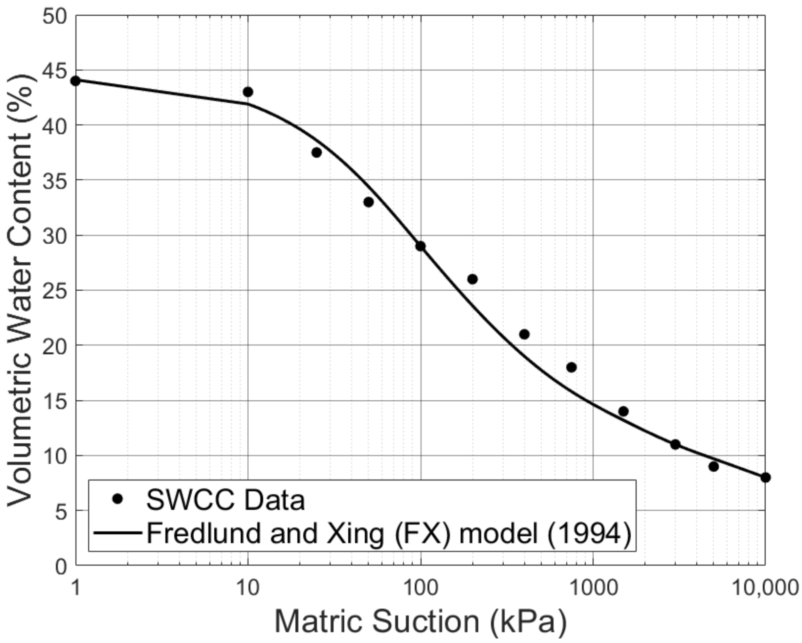

Figure 5. Soil–water characteristics curve of the soil plotted using Fredlund and Xing (1994) model [48].

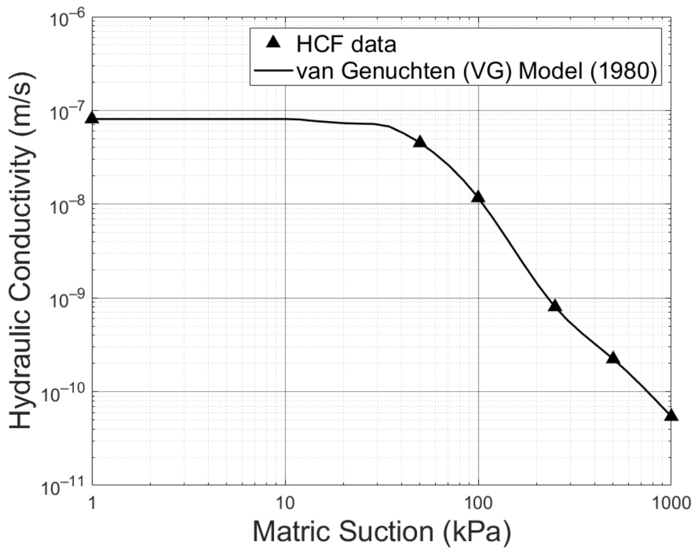

Figure 6. Hydraulic conductivity function of soil plotted using van Genuchten (1980) model [49].

Table 2. Soil properties used in the study.

Region	Soil Property	Value
Compacted fill/Surface layer	Dry unit weight (kN/m^3)	16.5
Compacted fill soil	Saturated Coefficient of Permeability, k_s (m/s) Cohesion, c (kPa) Angle of internal friction, φ (°)	8.1×10^{-8} 38 17
Surface layer (desiccated soil)	Saturated Coefficient of Permeability, k_s (m/s) Cohesion, c (kPa) Angle of internal friction, φ (°)	8×10^{-5} 0 27

3.2. Geometry of the Section

In this study, the steepest part of an embankment of expansive soil was considered for analysis. The cross-section of the slope with a steepness of 2.5 H:1 V is shown in Figure 7. The embankment has two parts: compacted fill soil and surface layer. The surface layer thickness of the slope is 1.1 m (3.6 ft). The slope has a height of 8.54 m (28 ft), and the ground water table is situated at 8 m on the right side and 4 m on the left side above the base of the embankment. A mesh convergence study was conducted on the embankment section with a non-fissured surface layer to obtain an optimum mesh size suitable for the study. The change in the factor of safety (FOS) with mesh size was considered. Based on the mesh convergence study, a mesh size of 0.8 m was considered for the analysis. The mesh structure of the embankment is illustrated in Figure 7. For better modeling of the fissured surface layer and estimation of flow through the surface layer, the surface layer of 1.1 m is modeled with four layers of finer mesh. The finite element analysis (FEA) model is scaled up in both the horizontal and vertical dimensions to prevent the influence of boundary conditions. The bottom boundary is considered to be rigid with no permissible movement in either direction, while the two lateral boundaries are free to move only vertically. The desiccated layer is considered for the 3 m wide shoulder provided at the top of the embankment.

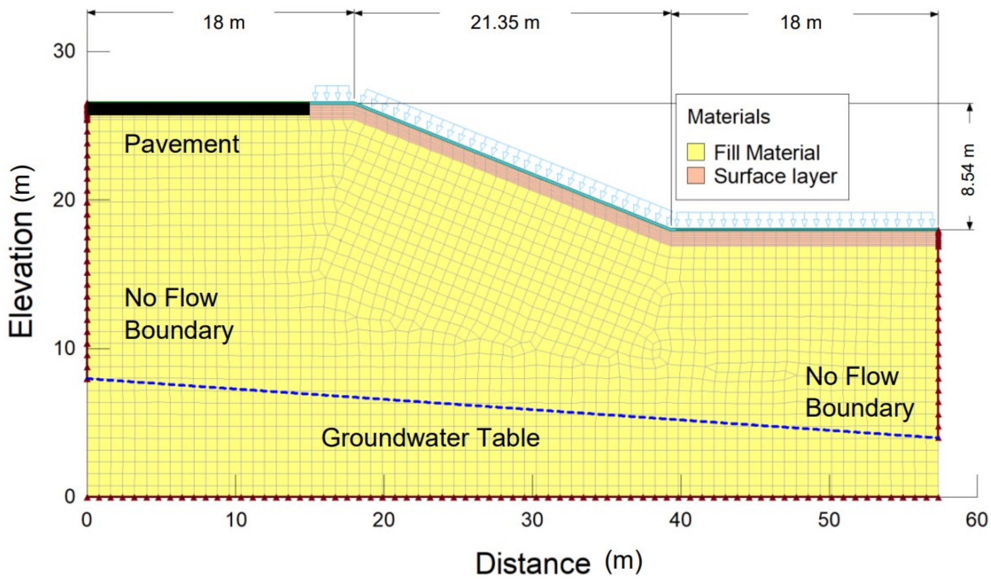

Figure 7. Profile and mesh structure of the embankment.

3.3. Numerical Modeling of Unsaturated Soil and Hydro-Geotechnical Behavior

A finite element transient variably saturated seepage analysis was performed using SEEP/W software to model the temporal and spatial distribution of pore water pressures within the embankments. The soil material model was considered to be in a saturated or unsaturated state to account for all types of soil characteristics. The flow through the soil in both saturated and unsaturated conditions was simulated in Geo-slope GeoStudio SEEP/W 2023.1.1 using Darcy's law. In unsaturated conditions, the changing hydraulic conductivity with matric suction or degree of saturation was considered by using the HCF curve from Figure 6. The partial differential equation that governs the calculation of flux for 2D transient flow is shown below:

$$\frac{\partial}{\partial x}\left(k_x\frac{\partial H}{\partial x}\right)+\frac{\partial}{\partial x}\left(k_y\frac{\partial H}{\partial y}\right)+Q=m_w\gamma_w\frac{\partial H}{\partial t} \tag{3}$$

where H is the total hydraulic head, k_x and k_y are the coefficient of permeability in the x (horizontal) and y (vertical) direction, respectively, Q is the boundary flux, and m_w is the storage curve slope.

In SEEP/W, Richard's (1931) equation was employed to accurately estimate the effect of unsaturated flow. The equation for 2D flow through pores can be written as follows [51]:

$$K\frac{\partial\theta}{\partial t}=\frac{\partial}{\partial x_i}\left[K\left(K_{ij}^A\frac{\partial h}{\partial x_i}+K_{iz}^A\right)\right]-S \tag{4}$$

where h is the pressure head in the soil, θ is the volumetric water content, S represents the sink term, x_i are the coordinates, K_{ij}^A is the anisotropy tensor, and K is the hydraulic conductivity function.

The boundary conditions are illustrated in Figure 7. The flux boundary was used to simulate the rainfall intensity and duration and applied on the slope. The top portion of the slope is impermeable considering the presence of the pavement. No flow boundaries were considered on either the right or left side above the groundwater table, and the base of the profile was considered the no-flow boundary. The flux boundary for the precipitation was considered to be in a non-ponding condition; this prevented the accumulation of rainfall on the slope of the embankment.

At each time step of 0.5 h, SEEP/W simulated the seepage conditions, and that pore water pressure was used for the limit-equilibrium-based software, SLOPE/W 2023.1.1 analysis, which uses the Morgenstern–Price (1965) method to determine the factor of safety (FOS) of the slope [52]. The seepage conditions were imported from SEEP/W using a similar grid technique. The unsaturated shear strength was determined using the GeoStudio SLOPE/W program, which utilizes the extended Mohr–Coulomb failure model. This model provides two methods to incorporate the influence of matric suction on the shear strength of soil. The unsaturated shear strength is determined using two independent stress variables: the net normal stress and the matric suction. The method proposed by Vanapalli et al. (1996) was used to consider the unsaturated shear strength [53]. This method can be expressed as:

$$\tau=c'+(\sigma_n-u_a)\ tan\ \varphi'+(u_a-u_w)\left[\left(\frac{\theta_w-\theta_r}{\theta_s-\theta_r}\right)tan\ \varphi'\right] \tag{5}$$

where τ represents the unsaturated shear strength, c' is the effective cohesion, σ_n represents the total stress, φ' is the effective angle of internal friction, (σ_n-u_a) is the net normal stress, and (u_a-u_w) is the matric suction. The strength due to suction was incorporated into the limit equilibrium (LE) method employed by SLOPE/W. The factor of safety from the coupled hydro-geotechnical model obtained through the integration of the FE and LE methods was used as the indicator of the stability of the slope.

4. Results and Discussion

The impact of the changing climate on the embankment was evaluated with a variation of FOS from slope stability analysis conducted by coupled hydro-geotechnical modeling. Precipitation, among all other climatic parameters, has the most short-term destabilizing effect. As the embankment was built with expansive soil, due to swelling–shrinkage properties, desiccation cracks were found to occur. From the field data collected from the literature, the depth of the desiccated layer was 1.1 m. Considering the extreme events and the effect of drought, the coefficient of permeability was considered to be significantly higher by magnitude, as shown in Table 2. Due to rainfall infiltration, the desiccated zone parallel to the slope became saturated. For all cases, the slope was considered to have a desiccated surface.

The FOS results from SLOPE/W for the embankment for historical precipitation are shown in Figure 8. Figures 9 and 10 illustrate FOS with pore water pressure distribution for SSP2 and SSP5, respectively. The reduction in FOS can be seen for FC scenarios compared to the historical climate. Due to the increased precipitation intensity and coefficient of permeability of the surface layer, the FOS decreased further for extreme events. The FOS continuously decreased with the increasing intensity of precipitation, which was due to the reduction in the matric suction. In the "middle of the road" scenario, SSP2, the maximum rainfall intensity and the number of extreme precipitations does not increase significantly from the middle of the century to the end of the century. Thus, the change in FOS for the scenario with time is much less. However, for the higher gas emission scenario, SSP5–8.5, the decrease is significant at the end of the century as the number of extreme precipitation events and maximum daily precipitation both increase, which also increases the duration of future design storms significantly. The reduction in FOS for SSP5–8.5 compared to the historical climate from Figures 8 and 10 was found to be 19.5%. Figure 8 also shows the variation in PWP in the surface layer of the slope for historical precipitation. The higher PWP in the desiccated layer can be observed for extreme precipitation events. From the pore water pressure distributions for extreme events, the accumulation of percolated water between the desiccated layer and the non-desiccated layer can be observed. The intense precipitation and the difference between the coefficient of permeability may be the reason behind this accumulation. From Figures 8–10, it can be observed that with an increase in the intensity of precipitation and duration of the event, the accumulation increased. This may have facilitated the continued surficial failure.

The effect of climate change was estimated using transient seepage and slope stability analysis. The factor of safety of the slope was determined for each step with an interval of 30 min for a 24 h precipitation event. The degradation of FOS with time is shown in Figure 11. The reduction in the matric suction of the soil due to rainfall could have been attributed to the reduction in the stability of the slope.

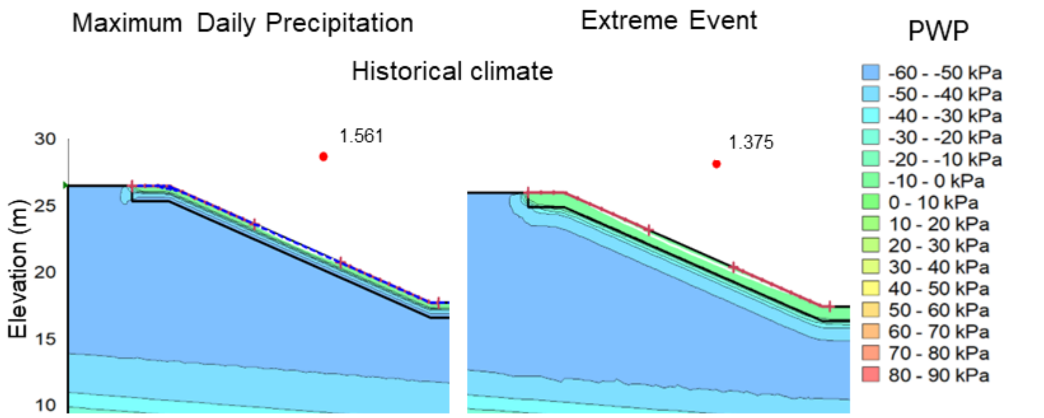

Figure 8. FOS with PWP distribution at the end of the precipitation event for the different scenarios for historical data.

It can be observed that, initially, the FOS was more than 3.5 and the value was stable for the initial hours for every scenario. With time, rainwater permeated further inside the embankment and reduced the matric suction, which eventually decreased the unsaturated shear strength. The intense rainfall generated the high pore water pressure early in the surface layer. The infiltration of rainfall in the desiccated layer caused the rapid degradation of FOS with time, mostly after 12 h of rainfall. The accumulation of water between the two layers discussed earlier could be the reason behind this rapid degradation of the stability of the slope.

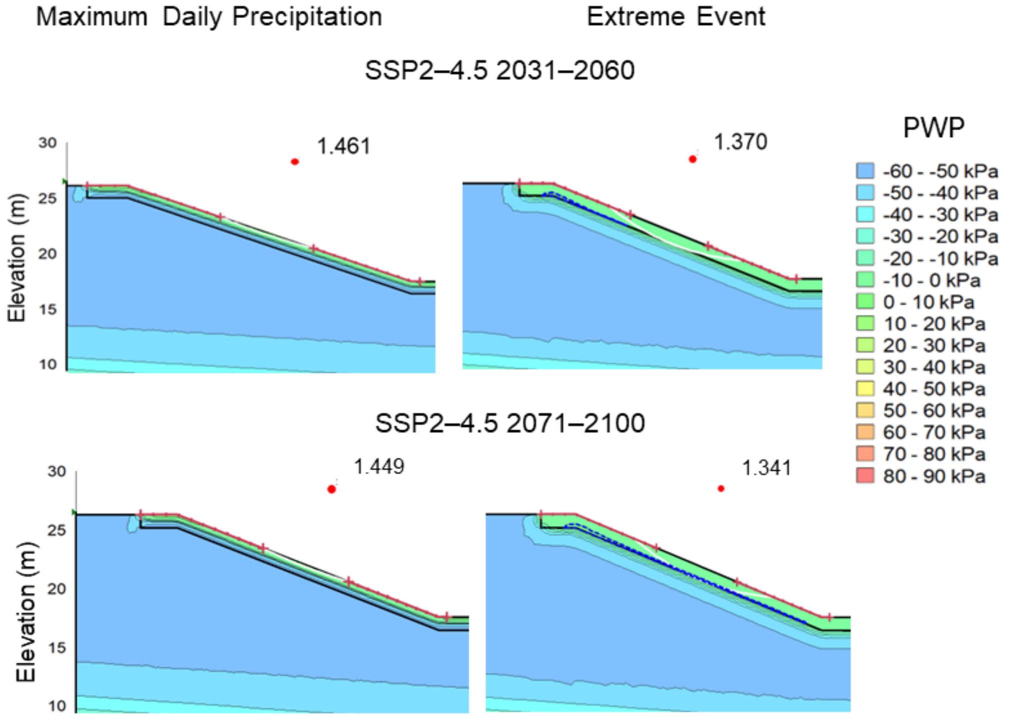

Figure 9. FOS with PWP distribution at the end of the precipitation event for the different scenarios in the future for SSP2–4.5.

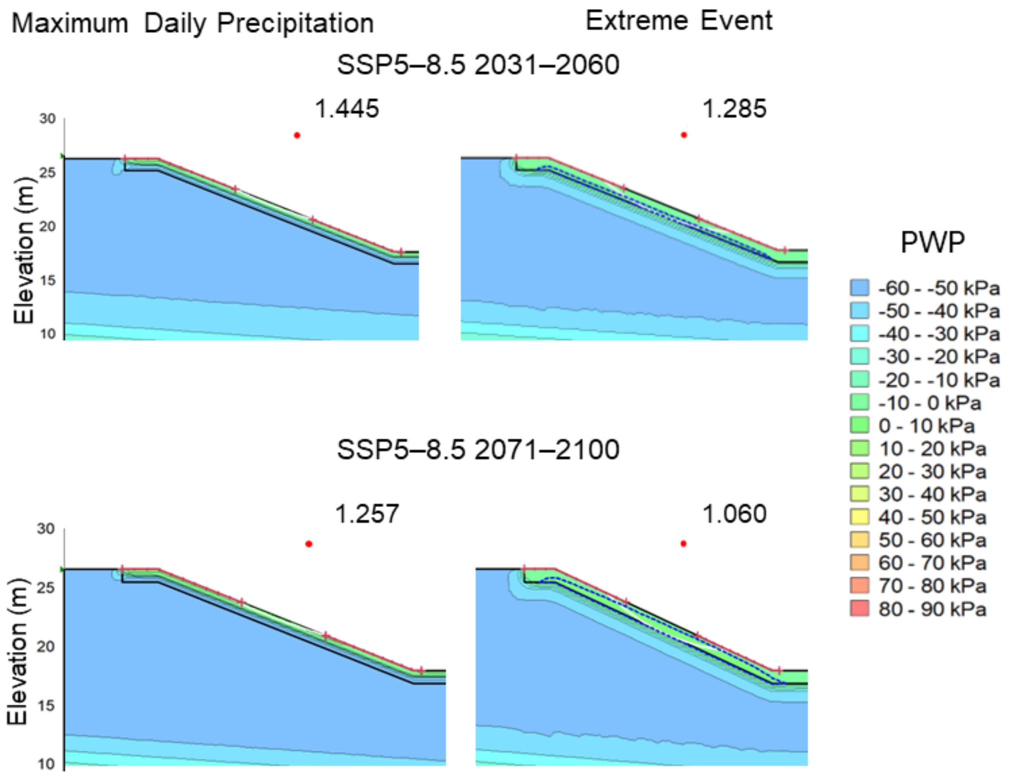

Figure 10. FOS with PWP distribution at the end of the precipitation event for the different scenarios in the future for SSP5–8.5.

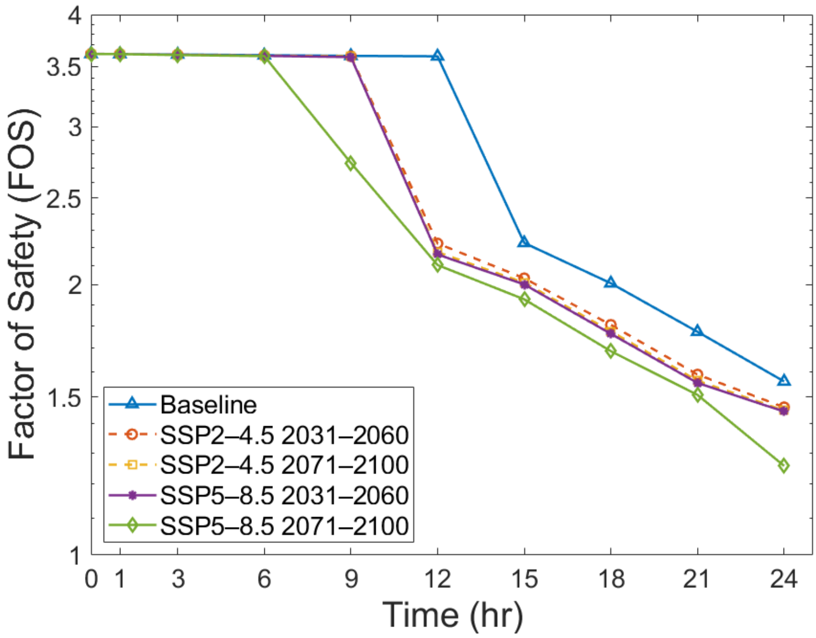

Figure 11. Change in FOS with temporal variations for 24 h precipitation for the baseline and future climate.

5. Conclusions

In this study, the impact of changing climate on the stability of earth embankments built with expansive soil in North Central Texas was numerically analyzed. The main focus of the study was to investigate the effect of the change in precipitation imparted due to climate change and the formation of desiccated layers due to the swell–shrink characteristics of the soil. The important observations of the study are as follows:

- Slopes built with expansive soil tend to form desiccation cracks due to swelling and shrinkage with climatic interactions. In the study, the stability of the slope was found to be reduced due to the formation of the desiccated surface layer.
- A 23% increase in the maximum daily precipitation and a 31.25% increase in the number of extreme precipitation events for SSP5 at the end of the century compared to historical precipitation between 1981 and 2010 was observed. In the future, the intensity of precipitation is predicted to be higher, with shorter intervals between the occurrence of extreme precipitation events.
- The stability analysis of the slope was conducted for two different SSPs: one with moderate greenhouse gas emissions and the other one with extreme GHG emissions with no emission control. The stability of the slope was predicted to be dependent on the greenhouse gas emission scenarios as it directly impacts the number of extreme precipitation events and the amount of daily precipitation.
- For both scenarios, two 30-year periods from the middle and end of the century were considered. With progress in the future, the FOS of the slope was predicted to be lower, and this reduction was significant for the extreme GHG emission scenario. The possibility of surficial failure was predicted to increase significantly for extreme events.

The influence of SSP5, which is an extreme scenario, on the precipitation intensity may be significant enough to induce the surficial surface of slopes with a desiccated top layer for other earthen embankments as well. Additional studies need to be conducted to understand the impact of other parameters such as temperature and solar radiation for different scenarios of climate change to quantify the potential impact of climate change on the resilience of earthen structures in different regions. Subsequently, sustainable measures need to be investigated and implemented to mitigate such issues by the end of the century. The incorporation of thermal and environmental stresses caused by climate change should be considered in the design of new structures, as such change is expected to have a negative impact on earthen infrastructures like dams, levees, and pavements throughout their lifespan.

Author Contributions: Conceptualization, A.B., P.K. and D.G.; methodology, D.G., P.K. and A.B.; software, D.G. and P.K.; formal analysis, D.G.; resources, A.B. and A.J.P.; data curation, D.G.; writing—original draft preparation, D.G.; writing—review and editing, D.G., A.B. and A.J.P.; visualization, D.G. and A.B.; supervision, A.B. and A.J.P.; project administration, A.B.; funding acquisition, A.B. All authors have read and agreed to the published version of the manuscript.

Funding: This research was funded by the US Department of Transportation—University Transportation Consortium (UTC)—Mountain-Plains Consortium (MPC), grant number MPC-687.

Data Availability Statement: All of the relevant data and models used in the study have been provided in the form of figures and tables in the submitted article. The data are also available upon reasonable request.

Acknowledgments: The authors gratefully acknowledge the US Department of Transportation—University Transportation Consortium (UTC)—Mountain-Plains Consortium (MPC), who funded this study. Any findings, conclusions, or recommendations expressed in this study are those of the authors and do not necessarily reflect the views of the funding agency.

Conflicts of Interest: The authors declare no conflict of interest.

References

1. Vardon, P.J. Climatic Influence on Geotechnical Infrastructure: A Review. *Environ. Geotech.* **2015**, *2*, 166–174. [CrossRef]
2. National Research Council. *Abrupt Impacts of Climate Change*; National Academies Press: Washington, DC, USA, 2013; ISBN 978-0-309-28773-9. [CrossRef]
3. Leshchinsky, B.; Vahedifard, F.; Koo, H.B.; Kim, S.H. Yumokjeong Landslide: An Investigation of Progressive Failure of a Hillslope Using the Finite Element Method. *Landslides* **2015**, *12*, 997–1005. [CrossRef]
4. Alonso, E.E.; Gens, A.; Delahaye, C.H. Influence of Rainfall on the Deformation and Stability of a Slope in Overconsolidated Clays: A Case Study. *Hydrogeol. J.* **2003**, *11*, 174–192. [CrossRef]
5. Fredlund, D.G.; Rahardjo, H.; Fredlund, M.D. *Unsaturated Soil Mechanics in Engineering Practice*; John Wiley & Sons, Inc.: Hoboken, NJ, USA, 2012; ISBN 9781118280492.
6. Sherwood, P.T. Effect of Sulfates on Cement- and Lime-Stabilized Soils. *Highw. Res. Board* **1962**, *41*, 98–107.
7. Alonso, E.E.; Romero, E.; Hoffmann, C.; García-Escudero, E. Expansive Bentonite-Sand Mixtures in Cyclic Controlled-Suction Drying and Wetting. *Eng. Geol.* **2005**, *81*, 213–226. [CrossRef]
8. Puppala, A.J.; Punthutaecha, K.; Vanapalli, S.K. Soil-Water Characteristic Curves of Stabilized Expansive Soils. *J. Geotech. Geoenviron. Eng.* **2006**, *132*, 736–751. [CrossRef]
9. He, S.; Yu, X.; Banerjee, A.; Puppala, A.J. Expansive Soil Treatment with Liquid Ionic Soil Stabilizer. *Transp. Res. Rec. J. Transp. Res. Board* **2018**, *2672*, 185–194. [CrossRef]
10. Talluri, N.; Puppala, A.J.; Congress, S.S.C.; Banerjee, A. Experimental Studies and Modeling of High-Sulfate Soil Stabilization. *J. Geotech. Geoenviron. Eng.* **2020**, *146*, 5. [CrossRef]
11. George, A.M.; Banerjee, A.; Puppala, A.J.; Saladhi, M. Performance Evaluation of Geocell-Reinforced Reclaimed Asphalt Pavement (RAP) Bases in Flexible Pavements. *Int. J. Pavement Eng.* **2021**, *22*, 181–191. [CrossRef]
12. Puppala, A.J.; Banerjee, A.; Congress, S.S.C. Geosynthetics in Geo-Infrastructure Applications. In *Durability of Composite Systems*; Reifsnider, K., Ed.; Woodhead Publishing: Sawston, UK, 2020; ISBN 9780128182604. [CrossRef]
13. Khan, M.A.; Biswas, N.; Banerjee, A.; Puppala, A.J. Field Performance of Geocell Reinforced Recycled Asphalt Pavement Base Layer. *Transp. Res. Rec. J. Transp. Res. Board* **2020**, *2674*, 69–80. [CrossRef]
14. Das, J.T.; Banerjee, A.; Puppala, A.J.; Chakraborty, S. Sustainability and Resilience in Pavement Infrastructure: A Unified Assessment Framework. *Environ. Geotech.* **2022**, *9*, 360–372. [CrossRef]
15. Caballero, S.; Acharya, R.; Banerjee, A.; Bheemasetti, T.V.; Puppala, A.; Patil, U. Sustainable Slope Stabilization Using Biopolymer-Reinforced Soil. *Geo-Chicago* **2016**, *2016*, 116–126. [CrossRef]
16. Samuel, R.; Puppala, A.J.; Banerjee, A.; Huang, O.; Radovic, M.; Chakraborty, S. Improvement of Strength and Volume-Change Properties of Expansive Clays with Geopolymer Treatment. *Transp. Res. Rec. J. Transp. Res. Board* **2021**, *2675*, 308–320. [CrossRef]
17. Biswas, N.; Puppala, A.J.; Khan, M.A.; Congress, S.S.C.; Banerjee, A.; Chakraborty, S. Evaluating the Performance of Wicking Geotextile in Providing Drainage for Flexible Pavements Built over Expansive Soils. *Transp. Res. Rec. J. Transp. Res. Board* **2021**, *2675*, 208–221. [CrossRef]
18. Acharya, R.; Pedarla, A.; Bheemasetti, T.V.; Puppala, A.J. Assessment of Guar Gum Biopolymer Treatment Toward Mitigation of Desiccation Cracking on Slopes Built with Expansive Soils. *Transp. Res. Rec. J. Transp. Res. Board* **2017**, *2657*, 78–88. [CrossRef]

19. Banerjee, A. Response of Unsaturated Soils under Monotonic and Dynamic Loading over Moderate Suction States. Ph.D. Thesis, Department of Civil and Environmental Engineering, University of Texas at Arlington, Arlington, TX, USA, 2017.
20. Fredlund, D.G. The 1999 R.M. Hardy Lecture: The Implementation of Unsaturated Soil Mechanics into Geotechnical Engineering. *Can. Geotech. J.* **2000**, *37*, 963–986. [CrossRef]
21. Fredlund, D.G. The Stress State for Expansive Soils. In Proceedings of the 6th International Conference on Expansive Soils, Keynote Address, New Delhi, India, 1–4 December 1987; pp. 1–9.
22. Cho, S.E.; Lee, S.R. Evaluation of Surficial Stability for Homogeneous Slopes Considering Rainfall Characteristics. *J. Geotech. Geoenviron. Eng.* **2002**, *128*, 756–763. [CrossRef]
23. Rahardjo, H.; Lim, T.T.; Chang, M.F.; Fredlund, D.G. Shear Strength Characteristics of a Residual Soil with Suction. *Can. Geotech. J.* **1995**, *32*, 60–77. [CrossRef]
24. Saleh, A.A.; Wright, S.G. *Shear Strength Correlations and Remedial Measure Guidelines for Long-Term Stability of Slopes Constructed of Highly Plastic Clay Soils*; FHWA/TX-98/1435-2F; Texas Department of Transportation: Austin, TX, USA, 1997.
25. McCleskey, L.K.; Puppala, J.A.; Dronamraju, S.V.; Perrin, L. Remedial Measures Planned to Prevent Surficial Failures. *Proc. GeoEdmonton* **2008**, *8*, 21–24.
26. Rahardjo, H.; Ong, T.H.; Rezaur, R.B.; Leong, E.C. Factors Controlling Instability of Homogeneous Soil Slopes under Rainfall. *J. Geotech. Geoenviron. Eng.* **2007**, *133*, 1532–1543. [CrossRef]
27. Vahedifard, F.; Jasim, F.H.; Tracy, F.T.; Abdollahi, M.; Alborzi, A.; AghaKouchak, A. Levee Fragility Behavior under Projected Future Flooding in a Warming Climate. *J. Geotech. Geoenviron. Eng.* **2020**, *146*, 04020139. [CrossRef]
28. Robinson, J.D.; Vahedifard, F. Weakening Mechanisms Imposed on California's Levees under Multiyear Extreme Drought. *Clim. Chang.* **2016**, *137*, 1–14. [CrossRef]
29. Church, M.; Miles, M.J. Meteorological Antecedents to Debris Flow in Southwestern British Columbia; Some Case Studies. In *Reviews in Engineering Geology, Vol. VII—Debris Flows/Avalanches: Process, Recognition, and Mitigation*; Costa, J.E., Wieczorek, G.F., Eds.; Reviews in Engineering Geology; Geological Society of America: Boulder, CO, USA, 1987; Volume 7, pp. 63–80. ISBN 0-8137-4107-6.
30. Banerjee, A.; Puppala, A.J.; Hoyos, L.R.; Likos, W.J.; Patil, U.D. Resilient Modulus of Expansive Soils at High Suction Using Vapor Pressure Control. *Geotech. Test. J.* **2020**, *43*, 3. [CrossRef]
31. Banerjee, A.; Puppala, A.J.; Congress, S.S.C.; Chakraborty, S.; Pedarla, A. Recent Advancements in Predicting the Behavior of Unsaturated and Expansive Soils. In *Lecture Notes in Civil Engineering*; Patel, S., Ed.; Springer: Singapore, 2021; Volume 140, pp. 1–21.
32. Banerjee, A.; Puppala, A.J.; Congress, S.S.C.; Chakraborty, S.; Likos, W.J.; Hoyos, L.R. Variation of Resilient Modulus of Subgrade Soils over a Wide Range of Suction States. *J. Geotech. Geoenviron. Eng.* **2020**, *146*, 9. [CrossRef]
33. Kumar, P.; Banerjee, A.; Chandra, S.S.; Puppala, A.J. Effect of Future Extreme Precipitation on Expansive Soil Embankments. In Proceedings of the IFCEE 2021, Reston, VA, USA, 6 May 2021; American Society of Civil Engineers: Reston, VA, USA; pp. 255–266. [CrossRef]
34. Qi, S.C.; Vanapalli, S.K. Numerical Study on Expansive Soil Slope Stability Considering the Cracks and Coupling Effects. In *Unsaturated Soil Mechanics—From Theory to Practice, Proceedings of the 6th Asia-Pacific Conference on Unsaturated Soils, Guilin, China, 23–26 October 2015*; CRC Press: London, UK, 2015; pp. 621–628. [CrossRef]
35. Yang, R.; Xiao, P.; Qi, S. Analysis of Slope Stability in Unsaturated Expansive Soil: A Case Study. *Front. Earth Sci.* **2019**, *7*, 292. [CrossRef]
36. Qi, S.; Vanapalli, S. Stability Analysis of an Expansive Clay Slope: A Case Study of Infiltration-Induced Shallow Failure of an Embankment in Regina, Canada. *Int. J. Geohazards Environ.* **2015**, *1*, 7–19. [CrossRef]
37. O'Neill, B.C.; Lamarque, J.; Lawrence, D. Developing Climate Model Comparisons. *Eos Trans. Am. Geophys. Union* **2014**, *95*, 462. [CrossRef]
38. Almazroui, M.; Islam, M.N.; Saeed, F.; Saeed, S.; Ismail, M.; Ehsan, M.A.; Diallo, I.; O'Brien, E.; Ashfaq, M.; Martínez-Castro, D.; et al. Projected Changes in Temperature and Precipitation Over the United States, Central America, and the Caribbean in CMIP6 GCMs. *Earth Syst. Environ.* **2021**, *5*, 1–24. [CrossRef]
39. Committee on Adaptation to a Changing Climate. *Adapting Infrastructure and Civil Engineering Practice to a Changing Climate*; Olsen, J.R., Ed.; American Society of Civil Engineers: Reston, VA, USA, 2015; ISBN 9780784479193.
40. Robinson, J.D.; Vahedifard, F.; AghaKouchak, A. Rainfall-Triggered Slope Instabilities under a Changing Climate: Comparative Study Using Historical and Projected Precipitation Extremes. *Can. Geotech. J.* **2017**, *54*, 117–127. [CrossRef]
41. Pk, S.; Bashir, R.; Beddoe, R. Effect of Climate Change on Earthen Embankments in Southern Ontario, Canada. *Environ. Geotech.* **2019**, *8*, 148–169. [CrossRef]
42. Weisberg, S. *Applied Linear Regression*, 3rd ed.; John Wiley & Sons, Inc.: Hoboken, NJ, USA, 2005.
43. Chai, T.; Draxler, R.R. Root Mean Square Error (RMSE) or Mean Absolute Error (MAE)?—Arguments against Avoiding RMSE in the Literature. *Geosci. Model Dev.* **2014**, *7*, 1247–1250. [CrossRef]
44. Thrasher, B.; Wang, W.; Michaelis, A.; Melton, F.; Lee, T.; Nemani, R. NASA Global Daily Downscaled Projections, CMIP6. *Sci. Data* **2022**, *9*, 262. [CrossRef] [PubMed]
45. Giorgi, F.; Gao, X.-J. Regional Earth System Modeling: Review and Future Directions. *Atmos. Ocean. Sci. Lett.* **2018**, *11*, 189–197. [CrossRef]

46. *IPCC Climate Change 2021—The Physical Science Basis*; Cambridge University Press: Cambridge, UK; New York, NY, USA, 2021; ISBN 9781009157896.
47. Richter, I.; Tokinaga, H. An Overview of the Performance of CMIP6 Models in the Tropical Atlantic: Mean State, Variability, and Remote Impacts. *Clim. Dyn.* **2020**, *55*, 2579–2601. [CrossRef]
48. Fredlund, D.G.; Xing, A. Equations for the Soil-Water Characteristic Curve. *Can. Geotech. J.* **1994**, *31*, 521–532. [CrossRef]
49. van Genuchten, M.T. A Closed-Form Equation for Predicting the Hydraulic Conductivity of Unsaturated Soils1. *Soil Sci. Soc. Am. J.* **1980**, *44*, 892. [CrossRef]
50. Dronamraju, V.S. Studies on Field Stabilization Methods to Prevent Surficial Slope Failures of Earthfill Dams. Ph.D. Thesis, Department of Civil and Environmental Engineering, The University of Texas at Arlington, Arlington, TX, USA, 2008.
51. Richards, L.A. Capillary Conduction of Liquids through Porous Mediums. *Physics* **1931**, *1*, 318–333. [CrossRef]
52. Morgenstern, N.R.; Price, V.E. The Analysis of the Stability of General Slip Surfaces. *Géotechnique* **1965**, *15*, 79–93. [CrossRef]
53. Vanapalli, S.K.; Fredlund, D.G.; Pufahl, D.E.; Clifton, A.W. Model for the Prediction of Shear Strength with Respect to Soil Suction. *Can. Geotech. J.* **1996**, *33*, 2. [CrossRef]

Disclaimer/Publisher's Note: The statements, opinions and data contained in all publications are solely those of the individual author(s) and contributor(s) and not of MDPI and/or the editor(s). MDPI and/or the editor(s) disclaim responsibility for any injury to people or property resulting from any ideas, methods, instructions or products referred to in the content.